Journal of Structural Biology 187 (2014) 266–275

Contents lists available at ScienceDirect

Journal of Structural Biology

journal homepage: www.elsevier.com/locate/yjsbi

# 3D Raman mapping of the collagen fibril orientation in human osteonal lamellae

Susanne Schrof [a], Peter Varga [a], Leonardo Galvis [b,1], Kay Raum [a], Admir Masic [b,*]

[a] Julius Wolff Institute and Berlin-Brandenburg School for Regenerative Therapies, Charité Universitätsmedizin, Berlin, Germany
[b] Dept. of Biomaterials, Max Planck Institute of Colloids and Interfaces, Science Park Golm, 14424 Potsdam, Germany

ARTICLE INFO

*Article history:*
Received 12 May 2014
Received in revised form 4 July 2014
Accepted 5 July 2014
Available online 12 July 2014

*Keywords:*
Bone
Osteon
Polarized Raman spectroscopy
Chemical imaging
Collagen

ABSTRACT

Chemical composition and fibrillar organization are the major determinants of osteonal bone mechanics. However, prominent methodologies commonly applied to investigate mechanical properties of bone on the micro scale are usually not able to concurrently describe both factors. In this study, we used polarized Raman spectroscopy (PRS) to simultaneously analyze structural and chemical information of collagen fibrils in human osteonal bone in a single experiment. Specifically, the three-dimensional arrangement of collagen fibrils in osteonal lamellae was assessed. By analyzing the anisotropic intensity of the amide I Raman band of collagen as a function of the orientation of the incident laser polarization, different parameters related to the orientation of the collagen fibrils and the degree of alignment of the fibrils were derived. Based on the analysis of several osteons, two major fibrillar organization patterns were identified, one with a monotonic and another with a periodically changing twist direction. These results confirm earlier reported twisted and oscillating plywood arrangements, respectively. Furthermore, indicators of the degree of alignment suggested the presence of disordered collagen within the lamellar organization of the osteon. The results show the versatility of the analytical PRS approach and demonstrate its capability in providing not only compositional, but also 3D structural information in a complex hierarchically structured biological material. The concurrent assessment of chemical and structural features may contribute to a comprehensive characterization of the microstructure of bone and other collagen-based tissues.



## 1. Introduction

The remarkable mechanical properties of bone tissue are a result of the synergy of highly optimized material composition and complex hierarchical structure (Fratzl and Weinkamer, 2007; Weiner and Wagner, 1998). Lamellar bone is the most abundant type in the cortex of human bones. The basic building block of cortical lamellar bone is the osteonal lamella (OL) (Fig. 1a–c), a parallel layered structure with a thickness of 3–7 μm that is composed of a collagen fibril framework reinforced by mineral platelets and embedded in a mineralized extra-fibrillar matrix (Fig. 1d) (Fratzl and Weinkamer, 2007; Rho et al., 1998; Weiner and Traub, 1992; Weiner and Wagner, 1998; Granke et al. 2013). OL are concentrically disposed around a central Haversian canal forming characteristic structural motifs called osteons (Fig. 1c, e, f) (Rho et al., 1998). Among other material and structural factors such as tissue mineralization and collagen cross links, the fibrillar organization of OL is widely accepted to be the major determinant of the anisotropic elastic properties of osteonal tissue (Hofman et al., 2006; Koester et al., 2008; Reisinger et al., 2011; Wagner and Weiner, 1992). Therefore, better understanding of the fibrillar organization in OL provides further insights into the structure–function relationships of cortical bone tissue.

The fibrillar organization of OL has been the subject of numerous studies in the last decades. Nevertheless, the link between the fibrillar micro-architecture, chemical composition and resulting mechanical properties is still not fully understood and a multiplicity of models describing the fibrillar arrangements in OL has been proposed. Early investigations of the OL structure described the fibrillar alignment as (1) unidirectional with an abrupt change of orientation of 90° between adjacent lamellae (Gebhardt, 1906)

*Abbreviations:* OL, osteonal lamella; PRS, polarized Raman spectroscopy; 3D, three-dimensional; FWHM, full width at half maximum.

* Corresponding author. Fax: +49 331 5679402.
*E-mail address:* masic@mpikg.mpg.de (A. Masic).
[1] Present address: Aalto University, Forest Products Technology, Vuorimiehentie 1, 02150 Espoo, Finland.

http://dx.doi.org/10.1016/j.jsb.2014.07.001
1047-8477/

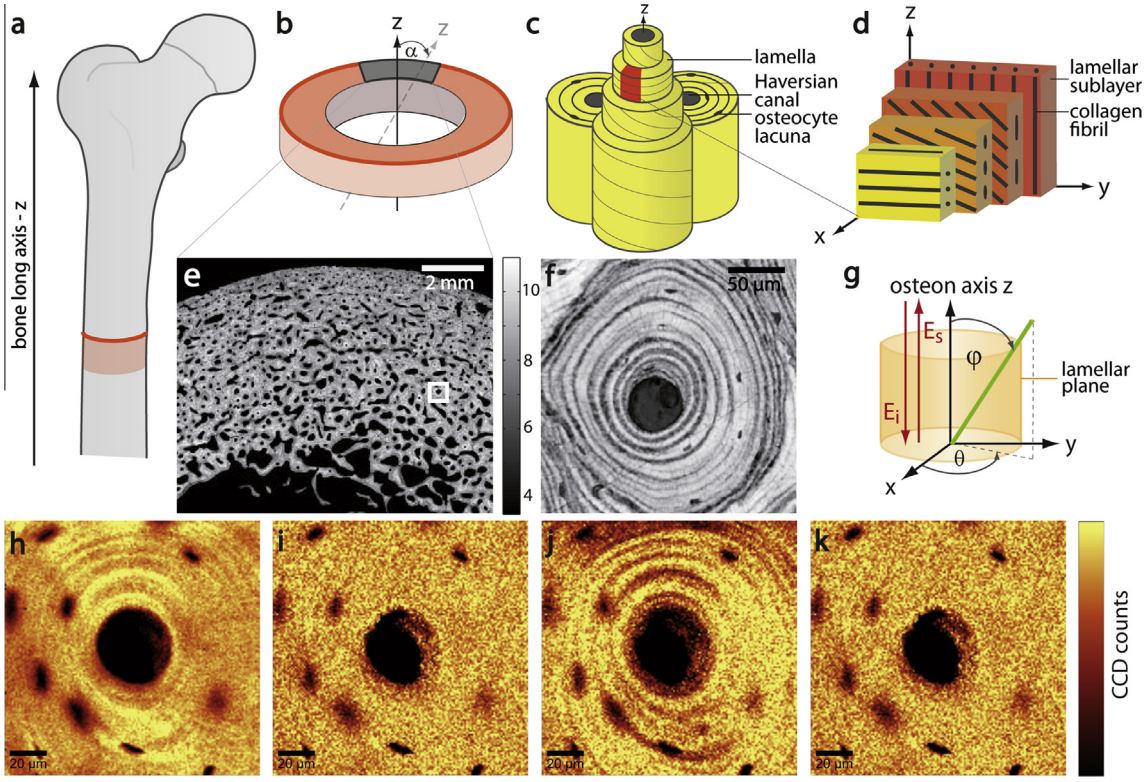


**Fig.1.** Summary and state of the art (a) Schematic drawing of a human proximal femur showing the location of the sample section in the diaphyseal region and the bone long axis z. (b) Schematic drawing of a cortical bone cross-section, illustrating the investigated sample surface plane (*xy* plane - orange). The gray area indicates the location where the acoustic microscopy scan in panel e was performed. (c) Osteons formed by lamellae concentrically disposed around a central Haversian canal and osteocyte lacunae. (d) Single bone lamella consisting of several sublayers of unidirectional aligned collagen fibrils. The *yz* plane is the lamellar plane; *x* is the axis perpendicular to the lamellar plane. (e) Acoustic impedance image scanned at 50 MHz showing an overview of lamellar bone tissue with its network of osteons (colorbar in MRayl). (f) Acoustic impedance image scanned at a frequency of 900 MHz illustrating the anisotropic mechanical properties of a single osteon (boxed region in panel e) with a central Haversian canal and osteocyte lacunae. (g) Definition of the global coordinate system and angles that describe the position and orientation of the collagen fibers. The direction of the incident and the scattered laser light are represented by the red arrows parallel to the *z*-axis. The lamellar plane is indicated. (h-k) Polarized Raman microscopy scans of a single osteon showing contrast images of (h) ν1 PO4 (CCD counts: 220–420) (i) ν2 PO4 (CCD counts: 50–160) (j) amide I (CCD counts: 40–155) (k) amide III (CCD counts: 25–80). The polarization direction of the incident laser light was horizontal (90°) in all images. ν1 PO4 and amide I reflect the characteristic lamellar structure of the tissue, due to their sensitivity to the orientation of the mineralized collagen fibrils; whereas ν2 PO4 and amide III are less susceptible to orientation effects and do not reflect the lamellar pattern, but show homogenous intensities in all osteonal regions(Kazanci et al., 2006).

or as (2) interwoven arrangements of fibrils in collagen-rich dense and collagen-poor loose layers (Marotti, 1993). Recent studies contradicted these first findings and demonstrated that the fibrillar arrangement in single lamella is neither unidirectional nor interwoven, but defined by particular fibrillar organization patterns. Each lamella is composed of several sublayers with unidirectional aligned fibrils and the fibril orientation varies depending on the position within the lamella (Fig. 1d). Various models describing these complex organization patterns have been established and quantitative description of the fibrillar orientation in the lamellar sublayers, the angles of tilt between adjacent sublayers and the sublayer thickness were reported. The proposed models include: (i) a twisted plywood pattern (Giraud-Guille, 1988; Giraud-Guille et al., 2003), characterized by a regular, continuous fibril rotation in the lamellar plane; (ii) an asymmetrical rotated plywood structure (Weiner et al., 1999; Weiner et al., 1997; Raum et al., 2011), defined by specific angles of tilt between lamellar sublayers of varying thickness, a characteristic "back-flip" phenomenon and different azimuthal rotations of the mineral platelets; (iii) a helicoidal plywood arrangement (Wagermaier et al., 2006) with a spiraling fibril orientation. Recently, (iv) coexisting oscillating, irregular oscillating and twisted plywood patterns with smooth orientation changes were identified. Furthermore, differences between highly organized and less regularly ordered lamellae were observed (Varga et al., 2013). More recent findings unite several of these model descriptions (v) and describe lamellar bone as a composite of ordered and disordered phases (Reznikov et al., 2013; Reznikov et al., 2014). The ordered phase is defined as mainly aligned fibrils arranged in twisted and oscillating plywood patterns, whereas the disordered phase is less densely packed and contains randomly oriented fibrils.

To provide detailed structural information of collagen fibrils and mineral platelets a wide range of analytical techniques have been applied. These include polarized light (Ascenzi and Bonucci, 1968; Giraud-Guille et al., 2003) and confocal microscopy (Ascenzi and Lomovtsev, 2006; Ascenzi et al., 2003), transmission and backscattered scanning electron microscopy (Giraud-Guille, 1988; Marotti, 1993; Weiner et al., 1991; Weiner et al., 1997), Fourier-transformed infrared (FTIR) microspectroscopy (Paschalis et al., 1996), small and wide angle X-ray scattering (SAXS and WAXS) (Fratzl et al., 2012; Wagermaier et al., 2006), dual beam electron microscopy (FIB-SEM) (Reznikov et al., 2013; Reznikov et al., 2014) and synchrotron X-ray phase nano-tomography (SR-PNT) (Varga et al., 2013; Langer et al. 2012). It is worth noting that most of these techniques require complex sample preparation and/or are unable to provide information in hydrated conditions, usually allow only small portions of the sample to be analyzed and do not provide correlative information on collagen and mineral.

Polarized Raman spectroscopy (PRS) emerges as a powerful non-destructive imaging tool which provides not only details on the chemical composition of bone tissue, but can furthermore be applied to obtain structural information of both collagen and mineral phase. Raman spectroscopy is based on the inelastic scattering of light when interacting with material, resulting in a frequency shift that can be associated with a particular vibrational mode of a specific chemical group. In bone research, Raman spectroscopy is a well-established method and is commonly applied to characterize the main tissue constituents, organic collagen and apatite mineral (Carden et al., 2003; Morris and Finney, 2004; Timlin et al., 1999). In addition to the chemical composition, the intensity of Raman scattering depends also on the orientation of the vibrational units with respect to the orientation of incident laser polarization. As a result, significant modulations of Raman peak intensities can be observed in highly structured biological tissues such as tendon or bone (Bonifacio and Sergo, 2010; Janko et al., 2010; Kazanci et al., 2006). Due to the specific arrangement of mineral platelets and collagen fibrils in bone, mineral ($\nu_1$ $PO_4$) and collagen (amide I) Raman peaks exhibit highly anisotropic and therefore modulated intensity responses (Carnelli et al., 2013; Falgayrac et al., 2010; Gamsjaeger et al., 2010; Makowski et al., 2013; Raghavan et al., 2010). However, in Raman microspectroscopic analysis it is crucial to distinguish between structurally and chemically related peak intensity modulations. In Fig. 1(h–k) an example of Raman microspectroscopic imaging of a human osteon using fixed orientation of laser polarization is shown. Clearly, the integrated intensities of mineral $\nu_1$ $PO_4$ ($\sim$960 $cm^{-1}$; Fig. 1h) and collagen amide I ($\sim$1660 $cm^{-1}$; Fig. 1j) bands show an intensity contrast that is originated from the characteristic organization of lamellar cortical bone (Kazanci et al., 2006). On the other hand, mineral $\nu_2$ $PO_4$ ($\sim$440 $cm^{-1}$; Fig. 1i) and collagen amide III ($\sim$1250 $cm^{-1}$; Fig. 1k) bands are less susceptible to the orientation effects and show an isotropic Raman response that qualifies these bands for analysis of bone composition (Falgayrac et al., 2010; Gamsjaeger et al., 2010; Gevorkian et al., 1984; Kazanci et al., 2006). It is worth noting at this point that, within the detection limits of spectral and spatial resolution, the total amount of phosphate ions ($\nu_2$ $PO_4$) and protein matrix (amide III) is constant throughout the entire osteon (except for the osteocytes regions) despite the complex structural organization (Kazanci et al., 2006; Hofman et al., 2006).

By acquiring spectral data at different orientations of the incident polarized laser light, the anisotropic Raman response of amide I can be used to derive information about the orientation of collagen molecules. Based on the anisotropic amide I response, Masic et al. (2011) determined the two-dimensional orientation of collagen fibrils in the plane perpendicular to the incoming laser beam (*xy* plane; Fig. 1g). Recently, Galvis et al. (2013) took first steps towards deriving three-dimensional (3D) orientation information of collagen molecules in tissues. Their work focused on the anisotropy of the theoretical Raman amide I band intensity of several collagen-like peptide structures and they established a model correlating the degree of anisotropy of the amide I response with an angle of orientation of the collagen molecules. Furthermore, 3D orientation information of collagen molecules in rat tail tendon (RTT) could be extracted by applying the theoretical model on experimental data. The aim of the present study is to extend the approach postulated by Galvis et al. from a simply structured tissue with mainly parallel aligned collagen fibrils to the analysis of a complex hierarchically structured collagen based tissue such as human cortical bone and assess 3D orientation of collagen fibrils in OL. We demonstrate that, additionally to the chemical composition, PRS is capable of elucidating intricate 3D mineralized collagen arrangements, including twisted and oscillating plywood patterns.

## 2. Materials and methods

### 2.1. Sample preparation

Four human femoral bone samples were obtained from human cadaver femora. All donors had no reported bone pathologies. Ethical approval was granted by Ethic Commission of the Martin Luther University. Cross-sectional samples were cut from the femoral mid-diaphysis. The samples were dehydrated in a graded series of ethanol (70%, 80%, 96% and 100%, immersion for 24 h each solution) and embedded in polymethylmetharylate (PMMA). Flat sample surfaces were prepared by a grinding procedure using silicon carbide abrasive papers (grit size 4000; Phoenix 4000, Buehler, Düsseldorf, Germany). Afterwards the surface was polished with a hard synthetic cloth, ethyleneglycol suspension and 1 μm diamond particles as an abrasive. Osteonal tissue sections for analysis were selected with scanning acoustic microscopy (SAM) as described elsewhere (Granke et al. 2013). SAM is a technique that quantifies acoustic impedance, which is strongly related to mechanical stiffness. SAM is thus sensitive to the elastic variations caused by the plywood pattern and can assess the lamellar structure of bone (Fig. 1f) (Hofman et al., 2006). Being not only non-destructive but also operating in backscattered geometry, SAM allows easy visualization of the lamellar structure of bone. Osteons were identified and selected based on their size, shape and lamellar structure.

### 2.2. Raman spectroscopy

For Raman microscopy a confocal Raman microscope (CRM200, WITec, Ulm, Germany) equipped with a piezo-scanner (P-500, Physik Instrumente, Karlsruhe, Germany), a diode pumped linearly polarized continuous 785 nm near infrared laser (Toptica Photonics AG, Graefelfing, Germany) and a water immersed objective 60× (NA = 1.00, Nikon, Tokyo, Japan) was used. The laser power was set to 30 mW and focused to a spot approximately 10 μm beneath the sample surface. The measured FWHM of the focal spot was ~1 μm in lateral direction and ~4 μm in axial direction. The Raman spectra were acquired using a CCD (PI-MAX, Princeton Instruments Inc., Trenton, NJ, USA) behind a grating (300 g $mm^{-1}$) spectrograph (Acton, Princeton Instruments Inc., Trenton, NJ, USA) with a spectral resolution of ~6 $cm^{-1}$. The sample surface was scanned in mapping mode with steps of 1 μm integrating the signal for 0.3 or 0.5 s at each step. The ScanCtrlSpectroscopyPlus software (version 1.38, WITec, Ulm, Germany) was used for the experimental setup and WitecProjectPlus software (version 2.02, WITec, Ulm, Germany) for spectral data processing. Chemical images were reconstructed by integrating over defined Raman shift regions in the spectrum using a sum filter (for amide I band the spectral region used was 1600–1700 $cm^{-1}$). Regions of interest (ROI) were scanned at different angles of polarization $\beta$ of the incident laser light in steps of $\Delta\beta = 15°$, from $\beta = 90°$ to $\beta = -90°$ with respect to the sample orientation. Collagen orientation maps were produced using built-in and custom-developed scripts in Matlab 7.5 (MathWorks Inc., Natick, MA, USA). For this, the following equation was fitted to the measured intensity variation of the amide I Raman band with respect to the polarization angle $\beta$

$$I = a(1 + b(cos(2(\beta - c)))) \quad (1)$$

where $I$ is the amide $I$ intensity response, $a$ the average amide I intensity of all scans, $b$ the amplitude of the fitting curve, $\beta$ the angle of polarization of the laser and $c$ the phase shift. These fit parameters are displayed in every *xy* scan position of the collagen orientation maps (Fig. 2): parameters *a, b*, and *c* are represented in color code of the pixel, length and orientation of the black arrows, respectively (Masic et al., 2011).

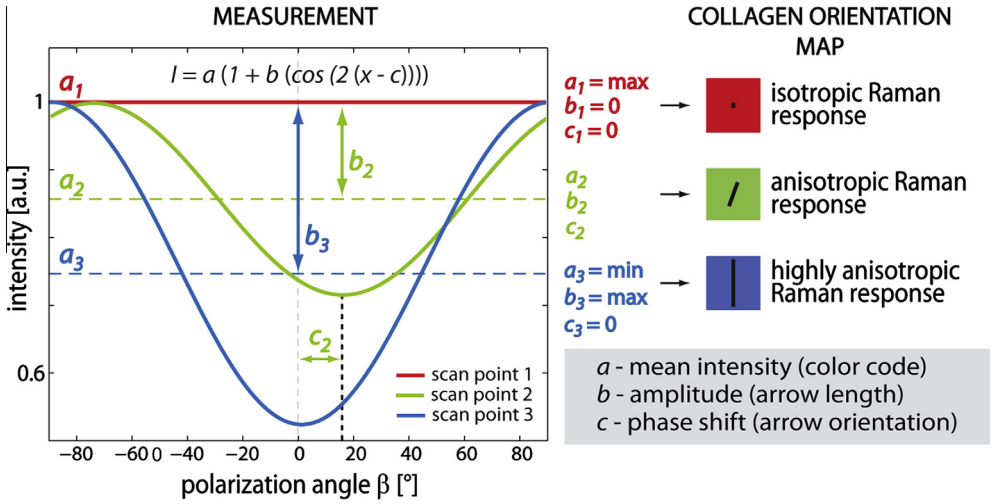


**Fig.2.** Illustration of the parameters of the fitting method and their visualization in collagen orientation maps. The graph shows the normalized intensity of the amide I Raman band of three hypothetical scan points measured at various angles of polarization β of the incident laser light. Parameter *a* (dashed lines), the mean amide I intensity of each scan point is represented in the color code of the pixel in collagen orientation maps. Parameter *b*, the amplitude of the fit of every scan point, which is determined by the degree of anisotropy of the Raman response, is represented in the length of the black arrows in collagen orientation maps and parameter *c*, the phase shift is represented by the orientation of the black arrows.

### 2.3. Modeling

To estimate and interpret the effects the misalignment between the incident laser beam and the lamellar plane due to oblique sample cutting and averaging of the fibril orientation as a result of the optical resolution, experimental data were compared to idealized theoretical models of the collagen fibril arrangement in OL. The lamellar structure of the osteon was modeled as plywood patterns. Single lamellae were defined as stacks of 25 sublayers of equal thickness. It was assumed that each sublayer is composed of unidirectional aligned collagen fibers. The arrangement of the fibrils in the lamella was modeled on the one hand as a twisted plywood pattern (Giraud-Guille, 1988) and on the other hand as an oscillating plywood pattern (Varga et al., 2013). Based on the results of Varga et al. (2013), a lamellar width of 7 μm was defined for all simulations. Furthermore, the twisted plywood model was defined by a continuous rotation of collagen fibrils from sublayer to sublayer with a twist angle of $\Delta\varphi = 7.5°$ between adjacent sublayers, corresponding to a twist rate of 25° per μm. The fibrils of the twisted plywood arrangement perform a full rotation from $\varphi = 0°$ to $\varphi = 180°$. The oscillating plywood pattern on the other hand was defined by fibrils that perform a sinusoidal oscillation between $\varphi = 0°$ and $\varphi = 30°$. (Schematic sketches illustrating side and top views of the two models are illustrated in Fig. 5(a, b, d, and e)). To evaluate the averaging effect of the focal domain, the confocal focus spot of the Raman microscope was modeled as a three dimensional Gaussian function with a full width at half maximum (FWHM) in *x*- and *y*-directions of 1 μm and a FWHM in *z*-direction of 4 μm.

## 3. Results and discussion

### 3.1. PRS resolves the 3D orientation of collagen fibrils in osteonal lamellae

PRS and imaging analysis was performed in osteonal tissue sections with characteristic lamellar structure. Fig. 3a provides a schematic overview of an osteon and shows an exemplary illustration of a region that was analyzed by PRS. Using the procedure reported in literature (Masic et al., 2011), a collagen fibril orientation map was derived (Fig. 3b). The map shows several OL and an osteocyte lacuna. The characteristic lamellar structure of bone is reflected in the oscillations of the mean amide *I* intensity. The measurement shows that the amide *I* Raman band in osteonal tissue exhibits a sinusoidal response with respect to the polarization angle *β*. The amplitude of this sinusoidal response (parameter *b*) reflects the degree of anisotropy of the PRS signal and varies depending on the position within the lamellae. Detailed analysis of the average values of single scan lines parallel to the lamellar plane (ROI 1a and ROI 1b, Fig. 3b) shows that the amide *I* response is isotropic in lamellar regions with local maximal mean amide *I* intensity (ROI 1a) and highly anisotropic in regions with a local minimal mean amide *I* intensity (ROI 1b). Comparison of the PRS response in the direction perpendicular to the lamellar plane (ROI 2, Fig 3c) shows a gradual increase of the degree of anisotropy from close to isotropic (ROI 2a) to highly anisotropic (ROI 2i).

In a theoretical study on collagen-like peptide molecules, Galvis et al. demonstrated that the degree of anisotropy of the amide *I* Raman response is determined by the orientation of the molecules. Their theoretical analysis predicted that the mean intensity of the amide *I* band is maximal and the response is isotropic, if the collagen-like molecules are parallel aligned with respect to the incident laser beam. On the other hand, molecules that are perpendicularly aligned to the incoming beam result in an anisotropic response with minimal mean amide *I* intensity. These predictions were furthermore verified in experimental investigations in rat tail tendon with highly oriented parallel collagen fibrils. It could be demonstrated that the degree of anisotropy is determined by the projection of the orientation of collagen fibrils in the *xz* plane (Galvis et al., 2013). Thus, it can be deduced that the gradual alteration of the anisotropy from isotropic to anisotropic in osteonal tissue, accompanied with the modulation of the mean intensity (Fig. 3, ROI 2), is caused by a continuous change of orientation of the collagen fibrils in the lamellar plane defined by an increasing twist angle $\varphi$. However, it is not possible to assign the mean amide *I* intensity/the degree of anisotropy to a specific twist angle $\varphi$ based on these data sets only.

To extract more information on the 3D orientation of the collagen fibrils, parameters *a*, *b*, and *c* and their correlation were further analyzed. The collagen orientation map in Fig. 4a provides details of several OL, the Haversian canal and two osteocyte lacunae.

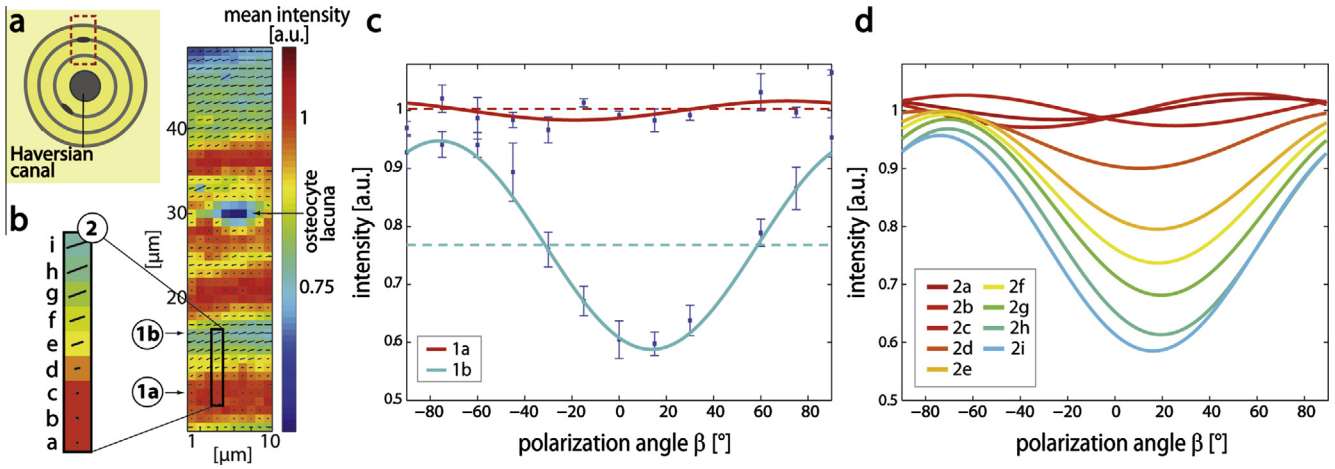


**Fig.3.** Amide I response of collagen fibrils in osteonal tissue. (a) Schematic overview of an osteon, the specific tissue section that was analyzed by polarized Raman spectroscopy is marked in dashed lines. (b) Collagen fibril orientation map showing several osteonal lamellae and one osteocyte lacuna. The map was obtained by fitting the amide I Raman band of 12 images collected at different angles of polarization of the incident laser light. Color code, length and orientation of the black arrows represent the average, normalized intensity of the amide I band, the amplitude of the corresponding fit and the fibril orientation in the *xy* plane, respectively. Representative ROIs (1a, 1b, 2) are marked. (c) Amide I intensity as a function of the angle of laser polarization. The plots show average and normalized amide I intensity values of two scan lines with local maximal (ROI 1a) and minimal (ROI 1b) amide I intensities in an osteonal lamella and their corresponding fits according to Eq. (1). Additionally, average amide I intensity values of the fits are shown (dashed lines). In regions with maximal intensities an isotropic amide I response (parameter *b* close to zero) can be observed. In contrast, in regions with minimal intensities the amide I response is highly anisotropic. (d) Comparison of the amide I responses of adjacent scan points in the direction perpendicular to the lamellar plane (ROI 2). It can be observed that the amide I response gradually becomes more and more anisotropic, as the average intensity decreases, reflecting increasing out of plane angles of the fibrils.

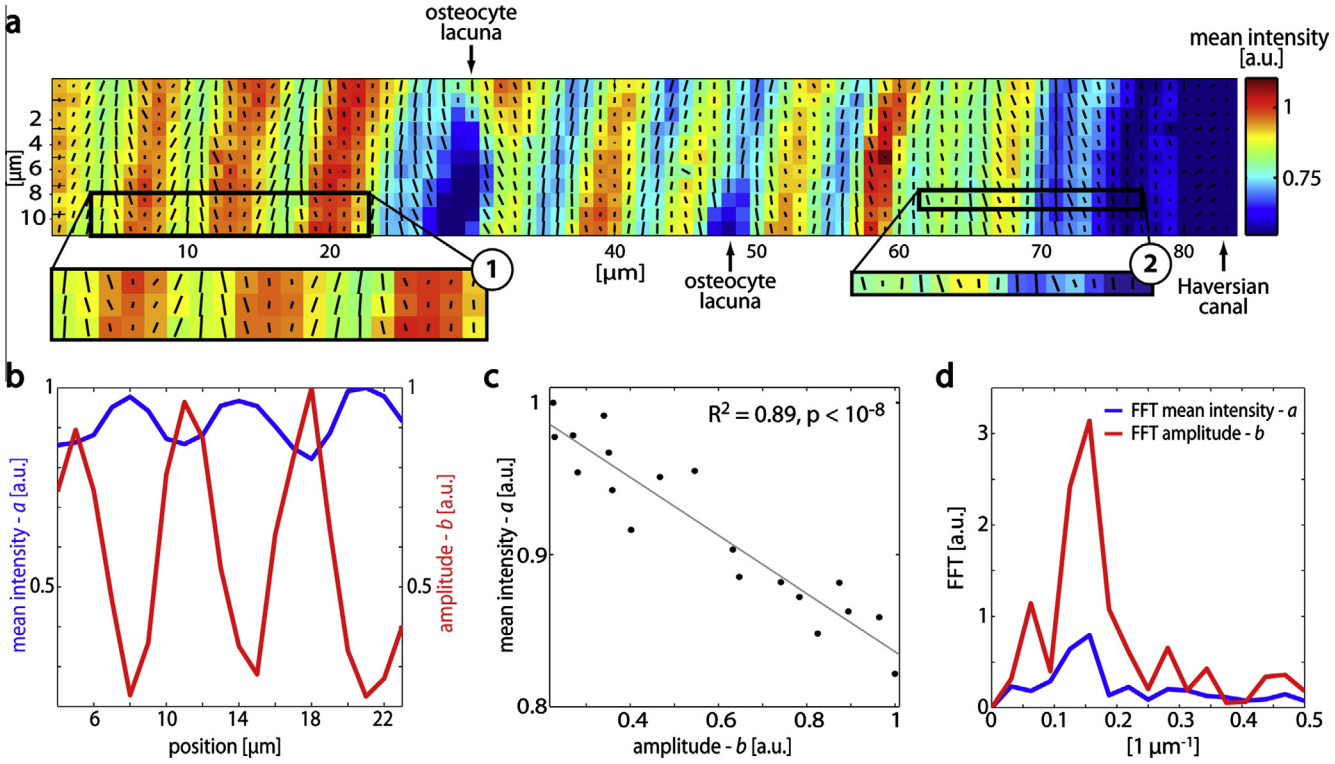


**Fig.4.** Collagen fibril orientation map of osteonal lamellae and analysis of fit parameters. (a) The map shows a subsection of an osteon with several osteonal lamellae (OL), the central Haversian canal and osteocyte lacunae. Representative ROIs are marked. (b) Mean values of the amide I intensity (parameter *a*, blue) and the amplitude of the fit (parameter *b*, red) of the scan lines of ROI 1 in panel a. The graphs illustrate the sinusoidal regression and negative correlation of the parameters. Both parameters reach a local maximum and minimum in every OL. (c) Linear regression analysis between average amide I intensity (red) and amplitude of the fitting curve (blue) of ROI 1 revealed a strong and negative correlation ($R^2 = 0.89$, $p < 10^{-8}$). (d) The fast Fourier transformation of the amide I intensity (blue) and the amplitude of the fitting curve (red) of ROI 1shows that the main components of the Fourier transforms of the two signals are in good agreement. The lamellar thickness corresponds to the oscillation period of both parameters and it results 6.5 µm in ROI 1. The phase difference between the maximum points of the two sinusoidal parameters is ~177°.

Analysis of the mean intensity (parameter *a*) and degree of anisotropy (parameter *b*) in representative ROIs proved that both parameters have a sinusoidal behavior across the OLs and are negatively correlated (Fig. 4b, c). Fast Fourier analysis of parameter *a* and *b* (Fig. 4d) revealed a mean phase difference of 178.3 ± 6.4° between maximum points of the two parameters in 9 representative OL. These results demonstrate that parameters *a* and *b* are in antiphase. The strong correlation between the mean amide *I* intensity and the degree of anisotropy in osteonal tissue is in good agreement with the theoretical predictions of collagen-like molecules (Galvis et al., 2013). Our findings provide evidence that the correlation between intensity and degree of anisotropy of the amide *I* response is not only valid for parallel aligned collagen fibrils, but also in a complex structure of fibrils with changing orientation.

There are several interesting aspects that emerge from these results. First and probably the most relevant, is that the parameter *b* is a reliable indicator for the orientation of the fibrils in the lamellar plane, parallel to the incoming laser beam. Earlier studies have shown that parameter *c*, the phase shift, represents the orientation of collagen fibrils in the *xy* plane, i.e. perpendicular to the incoming beam (Masic et al., 2011). Hence, these results show that 3D orientation information of collagen fibrils can also be extracted in a complex, highly mineralized biological tissue. In contrast to other techniques the PRS can also be applied to analyze fully hydrated collagen fibrils making this approach more relevant when it comes to assessing the tissue state that is as close as possible to the physiological conditions. Furthermore, the structural 3D orientation information can be in addition correlated to the chemical composition that is inherently incorporated into the Raman signal (e.g. water content, mineral phase characteristics, such as maturation or carbonation, nature of the organic matrix etc.) allowing for exploration of further structure–composition–function relationships in bone tissue.

### 3.2. Detection of different plywood arrangements in osteonal lamellae

Another interesting aspect found in collagen orientation maps is a periodic tilt of collagen fibrils out of the lamellar plane (e.g. ROI 2 in Fig. 3a-2, ROI 3 and 4 in Fig. 4a). Such a tilt has not been described in any of the reported osteonal models. However, (Giraud-Guille (1988)) observed series of nested arcs in their studies of compact osteonal bone and referred them to twisted plywood architecture in oblique sample sections. These nested arcs resemble the periodic tilts out of the lamellar plane observed with our PRS. To account for this phenomenon, we compared experimental results with theoretical simplified and idealized models of known lamellar patterns. Based on the oscillations of the anisotropy of the Raman response experimental data were compared to (i) the twisted plywood pattern and (ii) to the oscillating plywood pattern. 3D models of these two structures show that two patterns can be clearly distinguished in side view, but their projections in top view appear indistinguishable (Fig. 5b, e). Top view projections of both models show parallel aligned fibrils only, and no tilt with respect to the lamellar plane can be observed. However, these observations hold only for the ideal situation where the osteon axis is parallel to the incoming laser beam and the axis of observation (Fig. 5b, e). In reality, a slight tilt of the osteonal axis with respect to the bone long axis and/or an oblique cut of the sample with respect to the osteonal axis can occur. The tilted view by an angle of $\alpha = 10°$ was also simulated. As a result the projections of the fibrils *xy* plane appear tilted with respect to the lamellar plane (Fig. 5c, f). This is due to the fact that the collagen fibrils of each sublayer get cut at different twist angles. The projections of the fibrils at $\varphi = 45°$ and $\varphi = 135°$ in the twisted plywood pattern show opposite tilt angles whereas the analogue projections ($\varphi = 15°$ and $\varphi = 15°$) in the oscillating plywood pattern are inclined in the same directions. Very similar results were observed in the experimentally assessed collagen orientation maps suggesting an oblique cut of the osteonal tissue (Fig. 5g and h). The majority of investigated ROIs with oblique sectioning (Fig. 5g) displayed a fibril rotation pattern comparable to the twisted plywood model and a small number of ROIs in close proximity to the Haversian canal was comparable to the oscillating plywood pattern.

Besides the twisted and oscillating plywood pattern we observed single lamellae with remarkably thick sublayers (3–4 μm) of nearly unidirectional aligned fibrils parallel to the osteon axis (e.g. Fig. 3b, ROI 1a). These findings are in good agreement with structural motifs and features that have been found in human femoral bone (Reznikov et al., 2014; Varga et al., 2013), murine tibia (Reznikov et al., 2013) and equine metacarpal bones (Faingold et al., 2013) using other complementary experimental approaches.

### 3.3. PRS-based indications of disordered collagen fibrils

Finally, to explore the intrinsic heterogeneity of the osteonal tissue in relation to the presence of unordered collagen networks, the anisotropy (parameter *b*) of osteonal tissue was compared to the degree of anisotropy of theoretical predictions of collagen molecules and to experimentally outcomes of RTT (Fig. 6). Fig. 6a shows the maximum normalized amide I intensity of collagen-like peptide molecules as a function of the polarization of the incident laser of molecules oriented parallel to the incident laser beam ($\varphi = 0°$) and perpendicular to the laser light ($\varphi = 90°$) (Galvis et al., 2013). In comparison, Fig. 6b shows the amide I intensity of dry pre-stretched RTT ($\varphi = 0°$ and $\varphi = 90°$) and wet non-stretched RTT ($\varphi = 90°$) (Galvis et al., 2013; Masic et al., 2011). As illustrated in the table (Fig. 6d) the degree of anisotropy of the theoretical Raman response of collagen-like peptide molecules and dry pre-stretched RTT is very similar, whereas it is slightly smaller for wet non-stretched RTT confirming the bending of the collagen molecules in the gap region of collagen fibrils predicted from X-ray and molecular dynamics results (Buehler et al., 2011; Fratzl et al., 1998). Interestingly, the maximum degree of anisotropy obtained using the same procedure for the OL tissue results is remarkably lower (Fig. 6c, d) compared with both, pre-stretched dry RTT (∼45% decrease) and non-stretched wet RTT (∼30% decrease).

The loss in anisotropy observed for OL can be due to several reasons: (i) collagen fibrils never reach a configuration perpendicular to the incident laser beam ($\varphi = 90°$); (ii) the limited spatial resolution (∼1 μm in lateral and ∼4 μm in axial direction) of the experimental Raman setup that would yield to an averaged orientation values in the case the sublayer thickness is smaller than 1 μm and/or if the layer is tilted relative to the laser beam axis; (iii) an intrinsic disorder of the collagen fibrils in the lamellar sublayers.

For the identified twisted plywood patterns, in which a full twist from $\varphi = 0°$ to $\varphi = 180°$ has been observed, the first option (i) can be excluded.

The estimation of the resolution effect on the loss of anisotropy requires further analysis. The intensity response of each measuring point in OL is the result of the interaction of several lamellar sublayers with different orientations with the light of the focal spot. Considering the average thickness of a lamella, the focal spot of the Raman microscope with a lateral resolution of 1 μm could have relatively large effects on the intensity anisotropy. To quantify this influence the interaction of the laser spot volume with a bone lamella arranged in an ideal twisted plywood pattern was theoretically modeled (Fig. 7a). Based on the results of Varga et al. (2013) and on the oscillation period of parameter *a* and *b* in experimental Raman results (e.g. Fig. 4d, d) a lamellar width of 7 μm was assumed for these estimations. Because the projections of the

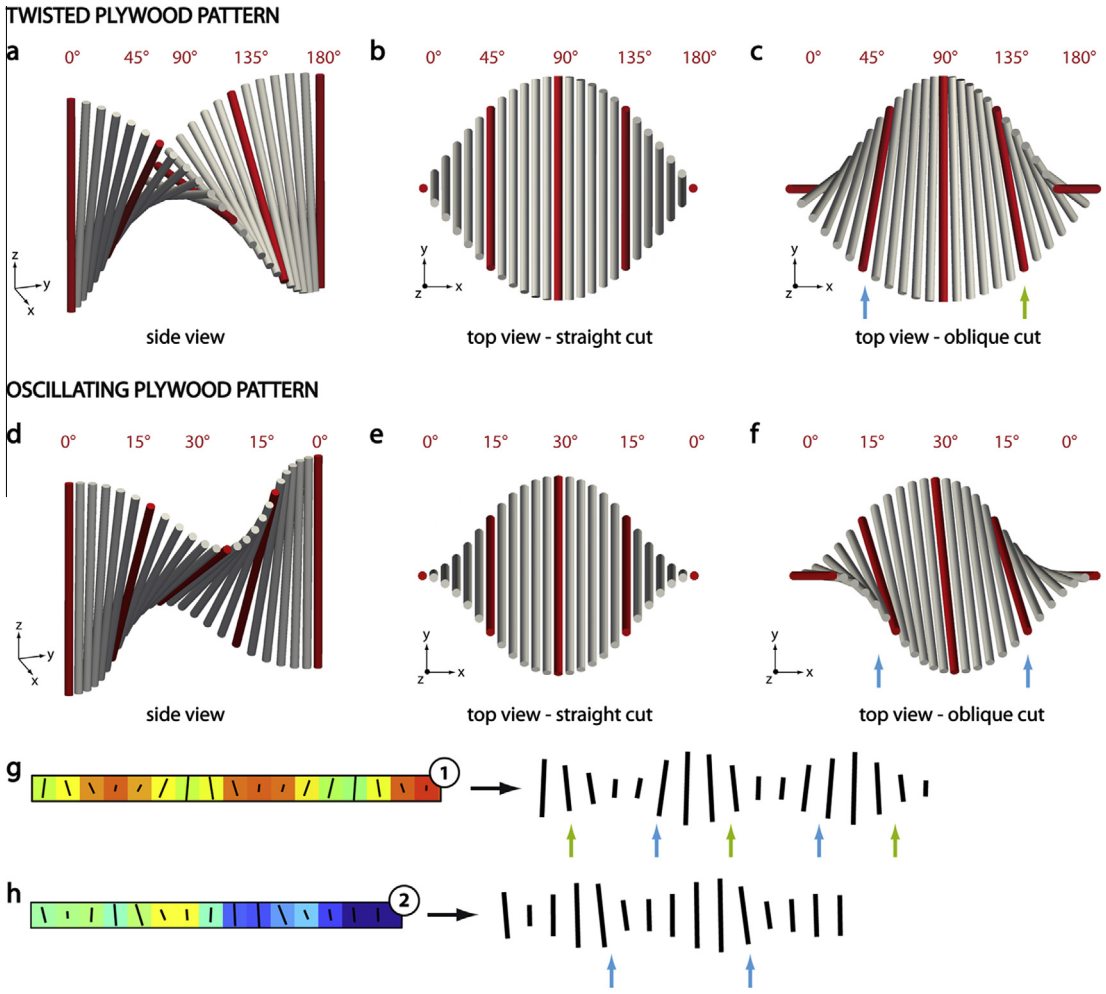


**Fig.5.** Schematic illustrations of different ideal plywood models and comparison with experimental data. Each panel illustrates the collagen fibril arrangement of a single bone lamella; every cylinder represents a sublayer of unidirectional aligned collagen fibrils. A lamellar thickness of 7 μm was assumed for both patterns. (a) Side view on a twisted plywood pattern: the fibrils continuously rotate clockwise from $\varphi = 0°$ to $\varphi = 180°$, the orientation of fibrils in adjacent sublayers is tilted by $\Delta\varphi = 7.5°$. The fibrils colored in red have a twist angle $\varphi$ of 0°, 45°, 90°, 135° and 180°. (b) Top view on a twisted plywood pattern cut perpendicular to the osteonal axis (straight cut). It can be observed that the projections of all fibrils are parallel and in the lamellar plane. (c) Top view on a twisted plywood pattern in an obliquely cut sample ($\alpha = 10°$). Due to the obliquely cut surface the projections of the fibrils appear to be rotated in the *xy* plane (blue and green arrow). The projections of the fibrils with $\varphi = 45°$ and $\varphi = 135°$ appear to have opposite rotation direction. (d) Side view on an oscillating plywood pattern. The fibrils perform a continuous sinusoidal oscillation from $\varphi = 0°$ to $\varphi = 30°$. The fibrils colored in red have a twist angle $\varphi$ of 0°, 15° and 45°. (e) Top view on an oscillating plywood pattern (straight cut). The projections of the fibrils appear to be parallel and in the lamellar plane. (f) Top view on an oscillating plywood pattern in an obliquely cut sample ($\alpha = 10°$). Due to the obliquely cut surface the projection of the fibrils appear to be rotated in the *xy* plane (blue arrows). The projections of the fibrils with $\varphi = 15°$ are rotated in the same direction. (g) Black lines indicate the collagen fibril orientation from one scan line of a collagen orientation map (extracted from ROI 1, Fig. 2a). It can be noted that the arrows are periodically rotated in the *xy* plane. Comparison of the experimental data with the plywood models shows good agreement with the twisted plywood pattern in an obliquely cut sample (blue and green arrows). (h) Black arrows from a scan line close to the Haversian canal (extracted from ROI 2, Fig. 2a). It can be observed that the arrows are periodically rotated in the *xy* plane. Comparison of the experimental pattern with the plywood models shows good agreement with the oscillating plywood pattern in an obliquely cut sample (blue arrows).

fibrils are measured only in *xy* plane, the PRS method is unable to distinguish between positive and negative twist angles in the lamellar plane based on parameter *b* only. Therefore the twisted plywood pattern was modeled as a continuous rotation from = 0° to $\varphi = 90°$ and back to $\varphi = 0°$. The focal laser spot was modeled as a 3D Gaussian distribution with a FWHM of 1 μm in *x*- and *y*-directions and a FWHM of 4 μm in *z*-direction. To estimate the effective twist angles measured with Raman microscopy, weighted mean twist angles of the fibrils within the focal volume were calculated (Fig. 7b). The estimation showed that the minimal and maximal twist angles are affected by the resolution of the microscope. Due to the averaging in the focal volume, the effective twist angles of collagen fibrils with predefined orientations of $\varphi = 0°$ and $\varphi = 90°$ in the model (parallel and perpendicular to the laser) were $\varphi^{\text{eff}} = 8°$ and $\varphi^{\text{eff}} = 82°$, respectively.

These estimations of the effective twist angles, that are even more pronounced in the models with oblique cutting (Fig. 7b), show that the effect of spatial resolution can account for at least two thirds of the loss of anisotropy of the OL in comparison to wet non-stretched RTT. It is worth noting that the effect of the resolution is crucially determined by the twist rate $\Delta\varphi$. Therefore this effect will have a much larger impact on lamellae with a twist rate $\Delta\varphi > 7.5°$. Consequently, it can be concluded that averaging of the twist angles as a result of the limited spatial resolution is one of the major reasons of the smaller *b* values (Fig. 6c) relative to the amide I Raman response of OL and compared to that of RTT (Fig. 6b) and

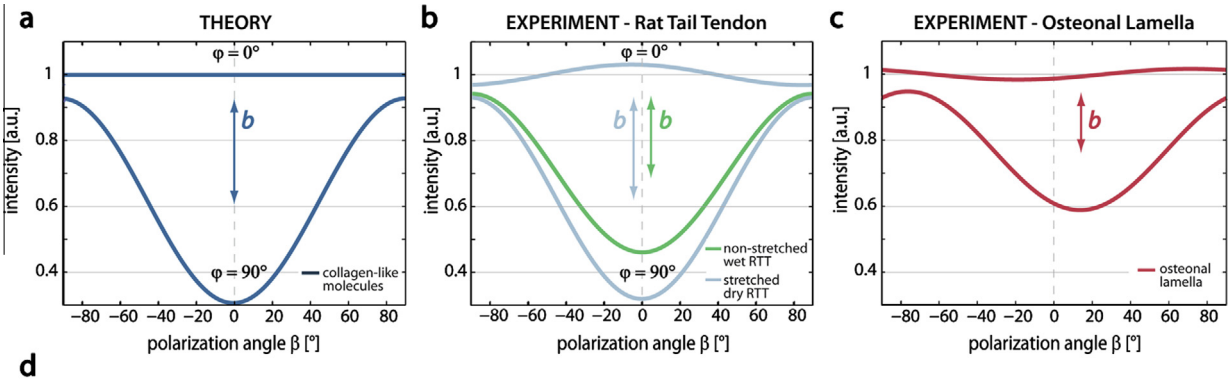


d

| | collagen-like peptide molecules | stretched dry rat tail tendon | non-stretched wet rat tail tendon | osteonal tissue |
|---|---|---|---|---|
| parameter *b* [a.u.] | 0.31 | 0.31 ± 0.03 | 0.24 ± 0.03 | 0.17 ± 0.01 |

**Fig.6.** Comparison of the amide I anisotropy degree of collagen-like molecules and different collagen-based tissues. (a) Average and normalized theoretical amide I response of four different collagen-like peptide structures that are rotated in the *xz* plane ($\varphi = 0°$) and ($\varphi = 90°$) vs the polarization angle of the incident laser light (Galvis et al., 2013). (b) Average and normalized experimental amide I response of non-stretched and pre-stretched rat tail tendon placed at the same angles as in (a) with respect to the incident laser light (Galvis et al., 2013; Masic et al., 2011). (c) Average and normalized experimental amide I response of the two regions in osteonal lamellae with the highest and lowest amide I intensity (Fig. 3b, ROI 1a and 1b) vs the polarization angle of the incident laser light. (d) Comparison of the theoretical prediction with the experimental data of rat tail tendon and osteonal tissue shows a clear loss in the degree of anisotropy (parameter *b*) in the experimental data, starting from the stretched RTT (comparable with the theoretical predictions), going through the unstretched RTT down to the lamellar tissue.

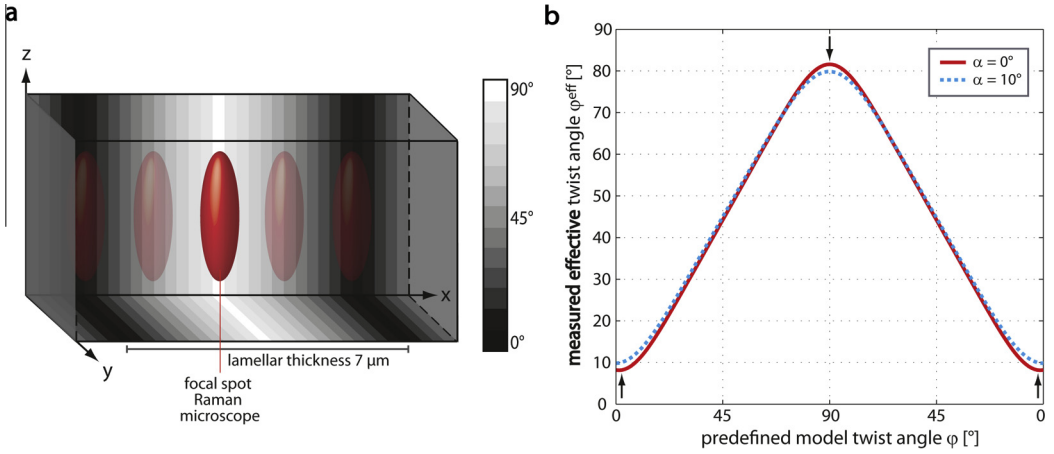


**Fig.7.** Simulation of the effect of the microscopic resolution on the measurement of the effective twist angle in lamellae. (a) Side view on a twisted plywood model with 25 sublayers with distinct collagen fibril orientation. A lamellar thickness of 7 µm and a twist rate of $\Delta\varphi = 7.5°$ between adjacent sublayers was assumed. The gray values represent the lamellar sublayers with twist angles $\varphi$. The focal spot of the Raman microscope is displayed in red. Due to the dimensions of the focal spot each spectral measurement is an interaction of the laser light of the focal spot with several sublayers of collagen fibrils with specific twist angles $\varphi$. (b) Comparison of the predefined angle of the twisted plywood model and estimation of the effective twist angle measured with Raman microscopy. The effective twist angle was estimated as the weighted mean value of the fibrils within the focal volume. Furthermore, effective twist angles in a twisted plywood model with oblique cut were estimated. As indicated with the black arrows, the effective minimal and maximal twist angles in the lamella are larger and smaller than the predefined model twist angles, respectively.

the theoretically predicted response of collagen-like molecules (Fig. 6a).

Ultimately, the anisotropy loss in OL may be associated to the presence of intrinsically disordered collagen fibrils. This structural feature has been postulated in several studies. Recently, Reznikov et al. (2013) observed, by means of a FIB-SEM method, the existence of thin disordered lamellar sublayers with loose fibril packing and little or no preferred orientation in the lamellar structure in rat circumferential bone and described a continuous disordered component enveloping a structure of highly ordered collagen fibrils in human osteonal bone (Reznikov et al., 2014). These findings were in line with recent findings of Varga et al. (2013) who found proof of specific regions with less regularly organized fibrils in a 3D study of lamellar bone using synchrotron X-ray phase nano-tomography. However, these studies report not only the presence of disordered sublamellar regions but also regions with highly organized collagen fibrils. In PRS analysis the loss of anisotropy in such regions should be limited. However, the magnitude of the degree of anisotropy never reached the experimental values of wet non-stretched RTT. This could be due to two possible reasons: (1) averaging of ordered and disordered lamellar sublayers as result of the limited spatial resolution or (2) equally distributed disordered collagen within the lamella. Even though the presence of disordered collagen results the most plausible explanation to

the loss of the anisotropy associated with the OL signal, the spatial resolution limitations of the PRS approach make the precise quantification and the contribution very difficult and error susceptible.

## 4. Conclusions

In summary, in this work we demonstrated the potential of PRS in assessing the 3D orientation patter of collagen fibrils in a highly complex hierarchically structured biological tissue. By analyzing the anisotropic response of the amide I Raman band of collagen fibrils in bone lamellae, evidence about the correlation between amide I intensity and degree of anisotropy of the Raman response in the complex and hierarchically structured tissue of osteons was provided. Based on this relation, information about the orientation of the collagen fibrils in the lamellar plane was derived. It could be demonstrated that the gradual change of anisotropy of the Raman response from isotropic to highly anisotropic is caused by the continuously increasing twist angle $\varphi$ of rotating collagen fibrils in OL. However, due to the limited resolution, the major drawback of the PRS methodology is its inability to precisely quantify the twist angle $\varphi$ of the collagen fibrils at a specific point in the tissue.

Based on apparent periodic tilts of the collagen fibrils out of the lamellar plane and comparison of the experimental data with theoretical models, two different collagen fibril arrangement patterns, the twisted and oscillating plywood pattern were identified in lamellae. Furthermore, the coexistence of both plywood patterns in the same osteon was observed, corroborating earlier findings. The majority of the lamellae displayed a twisted plywood pattern, but a small number of lamellae in close proximity to the Haversian canal displayed a fibril rotation comparable to the oscillating plywood pattern. Through the careful analysis of the amide I intensity plots, a loss of Raman intensity anisotropy in OL with respect to theoretical predictions and experimental data on RTT was observed. This loss in anisotropy was associated with (i) the averaging of twist angles as a result of the limited spatial resolution and (ii) the potential presence of disordered collagen fibrils within the lamellar organization.

Ultimately, the results reported here demonstrate the versatility of the PRS analytical approach to obtain collagen 3D structural information from a highly complex biological tissue, and concurrently map chemical information associated with collagen. In contrast to results reported in literature, PRS outcomes are based on the analysis of the fully mineralized and, in some cases, totally hydrated tissues, supporting the studies that involve the demineralization of the bone tissue prior to the structural characterization. In future, the methodology could provide further insights into the relationship between chemical composition, structural and mechanical properties of bone micro-mechanics. Finally, the proposed method could complement current diagnostic tools, as well as contribute to functional biomedical solutions for the assessment of tissue damage and response to treatment of collagen-related pathologies.

## Acknowledgments

This work was supported by the Deutsche Forschungsgemeinschaft (DFG, SPP1420, grants Ra 1380/7 and MA 6134/1-1).

## References

Ascenzi, A., Bonucci, E., 1968. The compressive properties of single osteons. Anat. Rec. 161, 377–391.
Ascenzi, M.-G., Lomovtsev, A., 2006. Collagen orientation patterns in human secondary osteons, quantified in the radial direction by confocal microscopy. J. Struct. Biol. 153, 14–30.
Ascenzi, M.G., Ascenzi, A., Benvenuti, A., Burghammer, M., Panzavolta, S., Bigi, A., 2003. Structural differences between "dark" and "bright" isolated human osteonic lamellae. J. Struct. Biol. 141, 22–33.
Bonifacio, A., Sergo, V., 2010. Effects of sample orientation in Raman microspectroscopy of collagen fibers and their impact on the interpretation of the amide III band. Vib. Spectrosc. 53, 314–317.
Buehler, M.J., Gautieri, A., Vesentini, S., Redaelli, A., 2011. Hierarchical structure and nanomechanics of collagen microfibrils from the atomistic scale up. Nano Lett. 11, 757.
Carden, A., Rajachar, R.M., Morris, M.D., Kohn, D.H., 2003. Ultrastructural changes accompanying the mechanical deformation of bone tissue: a Raman imaging study. Calcif. Tissue Int. 72, 166–175.
Carnelli, D., Vena, P., Dao, M., Ortiz, C., Contro, R., 2013. Orientation and size-dependent mechanical modulation within individual secondary osteons in cortical bone tissue. J. R. Soc. Interface 10, 20120953.
Faingold, A., Cohen, S.R., Reznikov, N., Wagner, H.D., 2013. Osteonal lamellae elementary units: lamellar microstructure, curvature and mechanical properties. Acta Biomater. 9, 5956–5962.
Falgayrac, G., Facq, S., Leroy, G., Cortet, B., Penel, G., 2010. New method for Raman investigation of the orientation of collagen fibrils and crystallites in the haversian system of bone. Appl. Spectrosc. 64, 775–780.
Fratzl, P., Weinkamer, R., 2007. Nature's hierarchical materials. Prog. Mater. Sci. 52, 1263–1334.
Fratzl, P., Misof, K., Zizak, I., Rapp, G., Amenitsch, H., Bernstorff, S., 1998. Fibrillar structure and mechanical properties of collagen. J. Struct. Biol. 122, 119–122.
Fratzl, P., Wagermaier, W., Gourrier, A., Burghammer, M., Kerschnitzki, M., Seidel, R., Gupta, H.S., 2012. Synchrotron 3D SAXS analysis of bone nanostructure. Bioinspired Biomimetic Nanobiomater. 1, 123–131.
Galvis, L., Dunlop, J.W.C., Duda, G., Fratzl, P., Masic, A., 2013. Polarized Raman anisotropic response of collagen in tendon: towards 3D orientation mapping of collagen in tissues. PloS One 8.
Gamsjaeger, S., Masic, A., Roschger, P., Kazanci, M., Dunlop, J.W.C., Klaushofer, K., Paschalis, E.P., Fratzl, P., 2010. Cortical bone composition and orientation as a function of animal and tissue age in mice by Raman spectroscopy. Bone 47, 392–399.
Gebhardt, W., 1906. Über funktionell wichtige Anordnungsweisen der feineren und gröberen Bauelemente des Wirbeltierknochens. II. Spezieller Teil. I. Der Bau der Haverśschen Lamellensysteme und seine funktionelle Bedeutung. Arch f Entwicklungsmechanik der Organismen 20, 187–322.
Gevorkian, B.Z., Arnotskaia, N.E., Fedorova, E.N., 1984. Study of bone tissue structure using polarized Raman spectra. Biofizika 29, 1046–1052.
Giraud-Guille, M.-M., Besseau, L., Martin, R., 2003. Liquid crystalline assemblies of collagen in bone and in vitro systems. J. Biomech. 36, 1571–1579.
Giraud-Guille, M.M., 1988. Twisted plywood architecture of collagen fibrils in human compact bone osteons. Calcif. Tissue Int. 42, 167–180.
Granke, M., Gourrier, A., Rupin, F., Raum, K., Peyrin, F., Burghammer, M., Saïed, A., Laugier, P., 2013. Microfibril orientation dominates the microelastic properties of human bone tissue at the lamellar length scale. PLoS One 8, 3.
Hofman, T., Heyroth, F., Meinhard, H., Fränzel, W., Raum, K., 2006. Assessment of composition and anisotropic elastic properties of secondary osteon lamellae. J. Biomech. 39, 2282–2294.
Janko, M., Davydovskaya, P., Bauer, M., Zink, A., Stark, R.W., 2010. Anisotropic Raman scattering in collagen bundles. Opt. Lett. 35, 2765–2767.
Kazanci, M., Roschger, P., Paschalis, E.P., Klaushofer, K., Fratzl, P., 2006. Bone osteonal tissues by Raman spectral mapping: orientation-composition. J. Struct. Biol. 156, 489–496.
Koester, K.J., Ager, J.W., Ritchie, R.O., 2008. The true toughness of human cortical bone measured with realistically short cracks. Nat. Mater. 7, 672–677.
Langer, M., Pacureanu, A., Suhonen, H., Grimal, Q., Cloetens, P., Peyrin, F., 2012. X-ray phase nanotomography resolves the 3D human bone ultrastructure. PLoS One 7, 8.
Makowski, A.J., Patil, C.A., Mahadevan-Jansen, A., Nyman, J.S., 2013. Polarization control of Raman spectroscopy optimizes the assessment of bone tissue. J. Biomed. Opt. 18, pp. 055005–055005.
Marotti, G., 1993. A new theory of bone lamellation. Calcif. Tissue Int. 53 (Suppl. 1), S47–55, discussion S56.
Masic, A., Bertinetti, L., Schuetz, R., Galvis, L., Timofeeva, N., Dunlop, J.W.C., Seto, J., Hartmann, M.A., Fratzl, P., 2011. Observations of multiscale, stress-induced changes of collagen orientation in tendon by polarized Raman spectroscopy. Biomacromolecules 12, 3989–3996.
Morris, M.D., Finney, W.F., 2004. Recent developments in Raman and infrared spectroscopy and imaging of bone tissue. Spectrosc – Int. J. 18, 155–159.
Paschalis, E.P., DiCarlo, E., Betts, F., Sherman, P., Mendelsohn, R., Boskey, A.L., 1996. FTIR microspectroscopic analysis of human osteonal bone. Calcif. Tissue Int. 59, 480–487.
Raghavan, M., Sahar, N.D., Wilson, R.H., Mycek, M.-A., Pleshko, N., Kohn, D.H., Morris, M.D., 2010. Quantitative polarized Raman spectroscopy in highly turbid bone tissue. J. Biomed. Opt 15, 037001.
Raum, K., Grimal, Q., Laugier, P., Gerisch, A., 2011. Multiscale structure–functional modeling of lamellar bone. Proc. Acoust. 9.
Reisinger, A.G., Pahr, D.H., Zysset, P.K., 2011. Elastic anisotropy of bone lamellae as a function of fibril orientation pattern. Biomech. Model. Mechanobiol. 10, 67–77.
Reznikov, N., Shahar, R., Weiner, S., 2014. Three-dimensional structure of human lamellar bone: the presence of two different materials and new insights into the hierarchical organization. Bone 59, 93–104.

Reznikov, N., Almany-Magal, R., Shahar, R., Weiner, S., 2013. Three-dimensional imaging of collagen fibril organization in rat circumferential lamellar bone using a dual beam electron microscope reveals ordered and disordered sub-lamellar structures. Bone 52, 676–683.
Rho, J.-Y., Kuhn-Spearing, L., Zioupos, P., 1998. Mechanical properties and the hierarchical structure of bone. Med. Eng. Phys. 20, 92–102.
Timlin, J.A., Carden, A., Morris, M.D., 1999. Chemical microstructure of cortical bone probed by Raman transects. Appl. Spectrosc. 53, 1429–1435.
Varga, P., Pacureanu, A., Langer, M., Suhonen, H., Hesse, B., Grimal, Q., Cloetens, P., Raum, K., Peyrin, F., 2013. Investigation of the three-dimensional orientation of mineralized collagen fibrils in human lamellar bone using synchrotron X-ray phase nano-tomography. Acta Biomater. 9, 8118–8127.
Wagermaier, W., Gupta, H.S., Gourrier, A., Burghammer, M., Roschger, P., Fratzl, P., 2006. Spiral twisting of fiber orientation inside bone lamellae. Biointerphases 1, 1–5.
Wagner, H.D., Weiner, S., 1992. On the relationship between the microstructure of bone and its mechanical stiffness. J. Biomech. 25, 1311–1320.
Weiner, S., Traub, W., 1992. Bone structure: from angstroms to microns. FASEB J. 6, 879–885.
Weiner, S., Wagner, H.D., 1998. The material bone: structure mechanical function relations. Ann. Rev. Mater. Sci. 28, 271–298.
Weiner, S., Arad, T., Traub, W., 1991. Crystal organization in rat bone lamellae. FEBS Lett. 285, 49–54.
Weiner, S., Traub, W., Wagner, H.D., 1999. Lamellar bone: structure–function relations. J. Struct. Biol. 126, 241–255.
Weiner, S., Arad, T., Sabanay, I., Traub, W., 1997. Rotated plywood structure of primary lamellar bone in the rat: orientations of the collagen fibril arrays. Bone 20, 509–514.